Structural, chemical, and electronic properties of the $Co_2MnSi(001)$/MgO interface

Roman Fetzer,[1,*] Jan-Peter Wüstenberg,[1] Tomoyuki Taira,[1] Tetsuya Uemura,[1] Masafumi Yamamoto,[1] Martin Aeschlimann,[2] and Mirko Cinchetti[2]

[1]*Division of Electronics for Informatics, Hokkaido University, Kita 14 Nishi 9, Sapporo 060-0814, Japan*

[2]*Department of Physics and Research Center OPTIMAS, University of Kaiserslautern, Erwin-Schrödinger-Straße 46, 67663 Kaiserslautern, Germany*

(Received 26 September 2012; published 17 May 2013)

The performance of advanced magnetic tunnel junctions built of ferromagnetic (FM) electrodes and MgO as an insulating barrier depends decisively on the properties of the FM/insulator interface. Here we investigate interface formation between the Co-based Heusler compound Co_2MnSi (CMS) and MgO by means of Auger electron spectroscopy, low-energy electron diffraction, and low-energy photoemission. The studies are performed for different annealing temperatures (T_A) and MgO layer coverages (4, 6, 10, 20, and 50 ML). Thin MgO top layers ($t_{MgO} \leqslant 10$ ML) show distinct surface crystalline distortions, which can only be partly healed out by annealing and, furthermore, lead to distinct adsorption of carbon species after the MgO surface is exposed to air. For $t_{MgO} > 10$ ML, the MgO layer surface exhibits clearly improved crystalline structure and hence only marginal amounts of adsorbates. We attribute these findings to MgO misfit dislocations occurring at the interface, inducing further defects throughout the MgO layer for up to at least 10 ML. Furthermore, spin-polarized photoemission spectra of the CMS/MgO interface are obtained for MgO coverages up to 20 ML, showing a clear positive spin polarization near the Fermi energy (E_F) in all cases.

DOI: 10.1103/PhysRevB.87.184418 PACS number(s): 85.75.−d, 68.35.Fx

I. INTRODUCTION

Magnetic tunnel junctions (MTJs) are prototypical spintronics devices, consisting of two ferromagnetic leads separated by an insulating barrier.[1–4] As first shown by Jullière, the resulting tunneling magnetoresistance (TMR) depends crucially on the electron spin polarization of the electrodes.[5] Therefore, the effectiveness of such devices can be increased significantly by using highly spin-polarized half-metallic materials. Amongst other predicted half metals, the Heusler compound Co_2MnSi (CMS) features a high Curie temperature of 985 K and proper epitaxial growth.[6–8] The predicted minority band gap[9–11] was experimentally demonstrated by tunneling spectroscopy at low temperature, having a width of approximately 400 meV, where the Fermi energy (E_F) lies very close to the conduction-band minimum.[8,12] Later studies confirmed the band-gap width, but found E_F in the middle of the minority band gap.[13] Indeed, a superior performance of CMS compared to conventional 3d ferromagnetic materials in MTJs using an amorphous AlO_x barrier could be demonstrated, at least for low temperatures.[14] However, perfect half metallicity only exists in theory, while at least small amounts of residual band-gap states are present in actual CMS films. Hence, further improvement was realized by using epitaxially grown MgO instead of AlO_x as the tunnel barrier.[8,15] As Butler *et al.* first predicted for Fe/MgO/Fe MTJs, the tunneling probability will depend additionally on the electron wave-function symmetry in the case of crystalline barriers due to $k_{||}$ conservation.[16] Using ferromagnetic materials with appropriate band structure, the preferential tunneling leads to significantly increased TMR ratios. This also holds for CMS/MgO/CMS MTJs.[17] Ishikawa and co-workers could raise the TMR value further, even above 1000%, by varying the chemical composition of CMS.[18]

Bulk MgO possesses a direct band gap at the Γ point.[19,20] The band-gap width is about 7.8 eV,[21,22] but can be reduced by defect-induced gap states[23–25] as well as surface states.[26,27] For MgO thin films, the band-gap width generally is reduced and depends on the fabrication procedure.[28–32] However, none of these cases leads to a finite density of states directly (±0.5 eV) at E_F, which usually falls in the middle of the MgO band gap. Epitaxial growth of MgO on top of CMS thin films inevitably leads to misfit dislocations at the interface due to the relatively large lattice mismatch of 5.1%.[33] Oxidation, as broadly discussed for the Fe/MgO interface, does not take place at the CMS/MgO interface in the case of electron-beam evaporation of the MgO layer.[34] In general, the performance of MTJs depends critically on heat treatment. Usually an optimum annealing temperature (T_A) for such devices has to be found, which results in a maximum TMR value.[35] For devices consisting of CMS and MgO, the optimum annealing temperature is in the range between 450 and 600 °C.[14,18,36]

In the past, a lot of effort has been put into characterization of MgO thin films grown on different metals. For example, Auger electron spectroscopy (AES) was performed on MgO thin films grown on metals in order to find out the surface chemical composition, i.e., whether stoichiometry is given[37] or interdiffusion takes place at the interface.[38] Other detailed investigations were done by low-energy electron diffraction (LEED) for Fe/MgO bilayers.[31,39,40] Pseudomorphic growth of MgO for up to 5–7 ML was found, resulting in sharp LEED spots. By overcoming the critical thickness, lattice-mismatch (3.5%) induced misfit dislocations occur at the interface, which lead to warped and tilted surface segments and increase surface roughness. In this case, the obtained LEED patterns consisted additionally of satellite spots with fourfold symmetry. For thicker MgO top layers, the tilting at the surface decreases; therefore, satellite and main spots smear out to single broad spots. Regarding the characterization of the spin-dependent electronic properties, up to now only the bare surface of different Heusler compounds has been investigated by spin-resolved photoemission spectroscopy (SR-PES).[41–47]

Applying this experimental technique to MTJ interfaces was done so far only for Fe/MgO, CoFe/MgO, and Co/MgO bilayers in order to reveal the electronic properties regarding spin and symmetry.[48–52] Due to the large band gap of MgO, Fe bulk states and possible interface states are, in principle, observable near E_F. However, in these studies, the MgO coverage could not exceed more than 2 ML. For thicker MgO coverage, due to the high surface sensitivity of conventional photoemission, the photoemission yield stems mainly from MgO. This, furthermore, results in a distinct drop of the detected surface spin polarization (SP).[32,53] Hence, the results can hardly be applied to MTJ properties, where the tunneling barrier usually has a thickness of at least 6 ML. Also pinholes cannot be excluded for such thin MgO layers ($\leqslant$2 ML), leading to a certain amount of metal surface contribution to the photoemission signal.

Here we investigate comprehensively the formation of the interface of advanced TMR devices consisting of half-metallic CMS and insulating MgO by means of LEED, AES, and low-energy SR-PES. These methods are applied to a set of CMS/MgO samples with varying MgO top layer thickness (t_{MgO}) ranging from 4 to 50 ML. For thin MgO coverages ($t_{\mathrm{MgO}} \leqslant 10$ ML), we find significant deviations of the crystalline ordering and elemental composition of the MgO surface. The spin-dependent electronic properties of the CMS/MgO interface are investigated directly via spin-resolved photoemission. This is possible by using a very low photon energy of $h\nu = 5.9$ eV.[54] A distinct positive spin polarization at E_F is found for MgO top layer thicknesses up to 20 ML, which drops monotonically for higher binding energies. All measurements on each of the samples were conducted in dependence upon the annealing temperature, ranging from 400 to 600 °C. We find that although the chemical composition of the MgO layers does not vary by annealing, strong changes appear for the thinner samples in crystal structure and photoemission spectra, again pointing out the influence of interface defects to the MgO top layer.

II. SAMPLES

The investigated samples were grown epitaxially in an ultrahigh vacuum chamber with a base pressure of 6×10^{-10} mbar.[55] The stack structure was the following: MgO(001)sub/MgO(10 nm)/CMS(30 nm)/MgO(x); $x = 4$, 6, 10, 20, and 50 ML, with 1 ML $\cong$ 0.211 nm. For the minimum MgO thickness, we have chosen $t_{\mathrm{MgO}} = 4$ ML (0.8 nm) since for thinner layers pinholes might occur. This would affect the investigated sample properties drastically, i.e., oxidation of the Heusler layer would take place when transferring *ex situ*. The CMS layer was evaporated by rf magnetron sputtering at room temperature (RT) and afterwards annealed up to 600 °C. The bulk chemical composition deviates from the stoichiometric case with an actual Mn-rich composition of $Co_2Mn_{1.19}Si_{0.88}$. MTJs using such Mn-rich compositions show distinctively improved TMR values up to a certain amount of manganese.[18] The MgO(001) top layers were deposited by electron-beam evaporation at RT. No additional annealing took place in the evaporation chamber. Layer thickness has been controlled by calibrated sputtering time (CMS) or by a quartz oscillator (MgO).[56] The samples were transferred *ex situ* to the experimental chamber and immersed into a non-water-containing liquid since MgO is known to be hygroscopic. Prior to the conducted experiments, the samples were annealed a second time via resistive heating in several steps from 400 up to 600 °C for at least 20 min, which allowed for systematic study of the dependence of the properties of the MgO layer as well as of the CMS/MgO interface on the annealing temperature (T_A). The actual temperature T_A was controlled by a calibrated Pyrometer measuring the sample holder surface temperature, with the Pyrometer spot directly beside the sample. The optimum annealing temperature for the CMS/MgO system is known to be 600 °C.[18,55]

III. EXPERIMENTAL SETUP

The setup of the experimental chamber is identical to the one described in detail by Wüstenberg *et al.*[42] LEED patterns of the samples were obtained by using a three-grid SpectaLEED system manufactured by Omicron. In all cases, a primary electron energy (E_P) of 90 eV was used to ensure high surface sensitivity. This allowed us to investigate the crystalline ordering degree of the outermost MgO surface layers. An Omicron CMA 100 energy analyzer in combination with an electron gun ($E_P = 3$ keV) was used for Auger electron spectroscopy, revealing the relative chemical composition of the MgO top layer surface.[57] For every species, a characteristic peak at a specific kinetic energy is evaluated, i.e., peak height and sensitivity factor (depends on element and energy) are taken into account to determine the element-resolved surface composition. The excitation source used for the photoemission experiments was the fourth harmonic of a Spectra Physics Tsunami Ti:sapphire oscillator with photon energy of 5.9 eV. The laser light was linearly p-polarized with an angle of incidence of 45 ° with respect to the surface normal. As given by the fcc crystal structure of CMS, this setup in general allows probing of electrons with Δ_1 and Δ_5 wave-function symmetries.[58] Please note that electronic bands having these symmetries are mainly responsible for the coherent tunneling current in MgO-based MTJs.[16,17] Photoelectrons leaving the surface in normal emission, i.e., the Γ-X direction, were detected by a 90 ° Focus CSA 300 cylindrical sector analyzer with an energy resolution of 210 meV.[42] Since the perpendicular component of the electron wave vector is not conserved during photoemission, the whole ΓX part of the Brillouin zone which is accessible with the used photon energy contributes to the photoemission spectrum. In this part, Δ_1 and Δ_5 majority bands cross the Fermi energy.[10,17] Additionally, due to the finite acceptance angle of our analyzer and further usage of a biasing voltage, we probe approximately 60% of the Brillouin zone in the Γ-K direction.[42] After energy detection, an additionally mounted Focus SPLEED analyzer is used to determine the spin asymmetry of the incoming photoelectrons. The actual spin polarization is calculated by using a Sherman factor value of 0.2. With this setup, a spin polarization of 30% is detected at E_F for a 200-nm-thick polycrystalline $Co_{70}Fe_{30}$ film. All experiments were carried out at room temperature.

IV. AES RESULTS

The AES spectra (not shown here) are, in general, dominated by Mg and O signals. For thinner MgO top layers, the elements of the underlying Heusler compound, i.e., Co, Mn, and Si, also contribute. For none of the samples is a distinct change of the chemical composition in dependence of the annealing temperature found, which means a significant interdiffusion at the interface does not take place at the investigated temperature range. Figure 1 shows the Mg:O ratio in dependence upon the MgO top layer thickness. The measured values are normalized to the bulk Mg:O ratio, which was obtained at a well-sputtered and heated MgO substrate. The data in Fig. 1 are obtained after annealing to 600 °C. While the samples with $t_{MgO} = 20$ and 50 ML show almost stoichiometric composition, the detected relative Mg amount decreases monotonically with respect to the oxygen signal for thinner coverages, reaching a minimum normalized ratio value of 16% for the sample with $t_{MgO} = 4$ ML. Valeri *et al.* observed a similar decrease of the Mg:O ratio when reducing the film thickness on top of silver from 20 down to 1 ML. They explained these findings by considering different electron inelastic mean free paths (IMFPs) for the evaluated O KLL (503 eV, $\lambda_{IMFP} \approx 13$ Å) and Mg KLL (1174 eV, $\lambda_{IMFP} \approx 25$ Å) peaks.[37,59] Therefore, the Mg signal apparently decreases because the respective λ_{IMFP} is in the range of the film thickness. Taking this effect into account, the right stoichiometry could be shown also for the thinnest MgO layers. However, this is not the case in our experiments, since even for a MgO thickness of only 1 ML, the apparent reduction of the Mg:O ratio due to IMFP effects would not exceed 50%, which is in contrast with our results. Please note that we did not fit the Mg:O ratio according to Ref. 37, since in our case we cannot assume a homogeneous film due to *ex situ* contaminations contributing to the O signal. Additionally, to the expected species, carbon was found on the surface of every sample, which probably originates from adsorption of carbon oxide molecules while the samples are exposed to air. This is inevitable since they are transferred *ex situ* to the experimental chamber. Remarkably, the relative C amount on top of the samples depends unambiguously on the MgO thickness, as can be seen from Fig. 1. For samples with $t_{MgO} = 20$ and 50 ML, the amount of C is negligible (values lower than 3%), while a clear monotonic increase occurs when going to lower MgO coverages resulting in a carbon amount of more than 20% for the thinnest MgO top layer thickness of 4 ML. It is well known that the perfect MgO surface is almost inert to molecular oxygen and carbon oxides, while adsorption of these species is likely to occur if point defects, steps, or terraces are present at the surface.[60–67] The enrichment of carbon oxides and molecular oxygen at the surface would furthermore result in an enhanced O signal, hence leading to the observed decrease of the Mg:O ratio. In conclusion, our observations point to a higher defect density at the MgO surface for lower MgO coverages. This behavior can be ascribed to misfit dislocations occurring at the CMS/MgO interface,[33] which can propagate to or at least induce defects and disorder at the MgO surface of samples with low MgO layer thickness, while for higher coverages the influence vanishes.

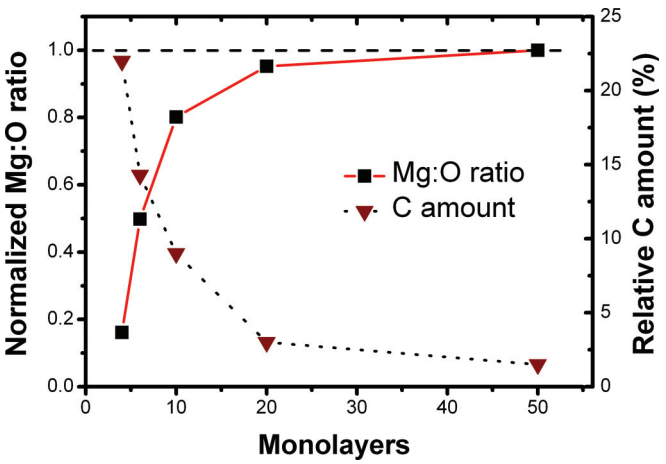

FIG. 1. (Color online) Mg:O ratio and relative carbon amount for varying MgO top layer thickness for CMS/MgO samples annealed at $T_A = 600$ °C. The connecting lines serve as a guide to the eye.

V. LEED RESULTS

LEED experiments were conducted on all samples in dependence upon the (second) annealing temperature T_A (400, 500, and 600 °C). For the sample with the thinnest MgO barrier (4 ML), a LEED pattern could not be observed, independently of T_A. The reason for the absence of diffraction spots may be the large amount of adsorbed carbon on the MgO surface, as found by AES (cf. Sec. IV). However, one has to keep in mind that the adsorption itself probably occurs due to a large defect density at the surface, which would also hinder the formation of a LEED pattern. For the samples with $t_{MgO} >$ 4 ML, we could observe the LEED pattern expected from the MgO B1 crystal structure.[42] In particular, for the samples with t_{MgO} =6 and 10 ML, we observed a significant improvement of the pattern quality by increasing T_A. This is illustrated in Figs. 2(a) and 2(b), showing LEED patterns obtained from the sample with $t_{MgO} = 10$ ML annealed to $T_A = 400$ °C and $T_A = 600$ °C, respectively. Here, an improvement of the pattern quality for higher annealing temperature is clearly visible. Since the chemical composition does not vary with T_A (cf. Sec. IV), we attribute this effect solely to the occurrence of defect healing throughout the whole MgO layer. Nevertheless, even for $T_A = 600$ °C, the spots are far from being sharp probably due to the presence of residual defects and adsorbed molecules at the surface.

In contrast to the previous behavior, the LEED patterns of the samples with $t_{MgO} = 20$ and 50 ML are hardly influenced

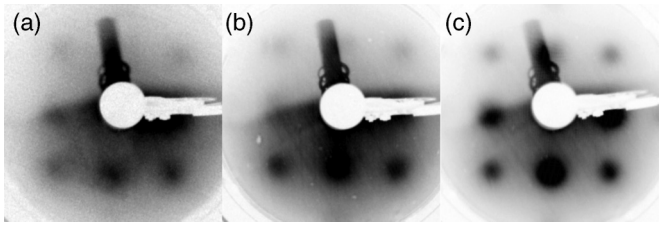

FIG. 2. LEED patterns at a primary electron energy of 90 eV of (a) $t_{MgO} = 10$ ML annealed to 400 °C, (b) $t_{MgO} = 10$ ML annealed to 600 °C, and (c) $t_{MgO} = 20$ ML annealed to 400 °C. Please note that the upper half of the luminescent screen is less sensitive.

by annealing. The obtained patterns have better quality compared to those recorded for lower MgO coverages, showing smaller spot widths and recognizable intensity differences. Figure 2(c) shows exemplarily the LEED pattern obtained from the sample with $t_{MgO} = 20$ ML and $T_A = 400\,^{\circ}$C, demonstrating that the LEED pattern quality is enhanced already for low T_A. Here the spot sizes are comparable to those reported in several other publications on nonmagnetic substrates and different MgO layer thicknesses.[37,68,69] Again, this can be explained by a diminished influence of the interface misfit dislocations to the sample surface in the case of higher MgO coverages, since less surface defects lead to an improved LEED pattern quality, while annealing effects are reduced. However, neither pointlike spots for very thin MgO layers induced by pseudomorphic growth nor additional satellite spots due to misfit dislocations occurring at thicker MgO coverages are found. This is in contrast to the protoype MTJ interface Fe/MgO,[31,39,40] which should be very comparable to the CMS/MgO interface since the lattice mismatch is similar and has the same sign. Our measurements suggest that pseudomorphic growth at the interface can only occur for $t_{MgO} < 4$ ML. In fact, for this type of growth, the MgO surface should be almost perfectly ordered and, therefore, no adsorption should take place. The satellite spots would be only observable in a certain layer thickness region, after exceeding the critical thickness and before the satellite spots and main spots blur due to the lowered surface tilting. The latter case cannot be excluded for the thicker MgO coverages of 20 and 50 ML (cf. Ref. 39). For the thinner MgO thicknesses, it is not possible to say if satellite spots occur or blurring already takes place since the LEED pattern quality is too low due to other surface defects and/or adsorbed species. Before continuing, we would like to stress that our results, indicating an imperfect MgO surface for typical MgO thickness used in TMR elements (6–10 ML), explain the fact that in TMR elements the upper CMS electrode usually grows worse compared to the lower one, leading to a decreased minority band-gap width and to residual bulk states in the gap itself.[13]

VI. SR-PES RESULTS

The work function of all samples is lower than the used photon energy of 5.9 eV, which, in principle, allows us to obtain spin-resolved photoelectron spectra in all cases. Although MgO is insulating, only the sample with the thickest MgO coverage of 50 ML shows charging effects, which cannot be overcome by reducing the laser intensity. Therefore, this sample will not be considered henceforth in this paragraph. We will start with a comparison of the results obtained after annealing to the optimal temperature of $T_A = 600\,^{\circ}$C. Figure 3 shows a comparison of the normalized (spin-integrated) spectra (bottom panel) and the corresponding spin polarization (SP, upper panel) for the samples with $t_{MgO} = 4$ and 20 ML ($T_A = 600\,^{\circ}$C). Both samples with intermediate MgO thickness ($t_{MgO} = 6$ and 10 ML) and $T_A = 600\,^{\circ}$C revealed spectra very similar to the one with $t_{MgO} = 4$ ML, while their SP values near E_F already reach the one of the 20 ML sample. The data in Fig. 3 show two very surprising facts: first of all, a nonvanishing spin polarization is detected despite the presence of a nonmagnetic MgO layer with thickness up

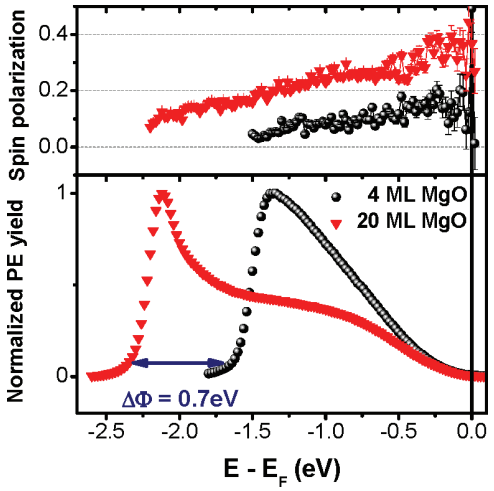

FIG. 3. (Color online) Spin-integrated and normalized spectra (lower part) and spin polarization (upper part) for samples with $t_{MgO} = 4$ and 20 ML with $T_A = 600\,^{\circ}$C.

to 20 ML on top of CMS; second, the photoemission yield does not drop significantly for thicker MgO coverages. Note that despite the photoemission yield decreases within the spectra towards E_F, the detected yield still allows one to determine the SP with enough accuracy (relative error on the SP at E_F is 5%). The origin of this unexpected behavior is the drastically reduced phase space for inelastic scattering of electrons excited at the CMS/MgO interface with MgO valence electrons because their excess energy ($\leqslant h\nu = 5.9$ eV) is smaller than the MgO band-gap energy of 7.8 eV.[21] As a result, the photoelectrons excited at the CMS/MgO interface do not significantly lose kinetic energy when traversing the MgO layer. This makes low-energy SR-PES sensitive to interfaces buried below insulator layers, as recently demonstrated in Ref. 54. Besides, hypothetic spin-polarized defects in the MgO layer itself cannot serve as an origin for the detected room temperature net spin polarization, since such defect spins are not able to align inside the nonmagnetic MgO matrix. Hence, in the literature, magnetic defects throughout the MgO layer have not been reported, although they would distinctively influence the TMR device properties.

By comparing the spin-integrated interface spectra in Fig. 3 to those of the free off-stoichiometric CMS surface in Ref. 42 and those from the free stoichiometric CMS surface in Ref. 54, we observe that in the CMS/MgO interface spectra, the spectral features are washed out. This is due to inelastic scattering at defects mostly at the very MgO surface region. This effect is even more pronounced than previously reported in Ref. 54, as, in contrast to Ref. 54, here the MgO surface was not sputter cleaned before the photoemission experiments. Scattering at the MgO surface affects almost all excited electrons and leads to a diminished photoemission yield at the Fermi edge. At lower energies, the spectra and the resulting spin polarizations are significantly influenced by secondary electrons which lost kinetic energy through scattering, hence leading to a monotonic increase of the photoemission yield and monotonic decrease of the SP. For this reason, only the spin polarization directly at E_F resembles the true interface spin polarization. Here we always find a distinct positive value, in contradiction

to several theoretical investigations which report large additional minority electron density at the CMS/MgO interface induced by hybridization,[17,70,71] resulting in a very low or even negative interface SP. Although these interface states should be detectable by our experimental setup, we attribute the missing of according features to the inevitable existence of lattice-mismatch-induced defects at the very interface, which prevents the formation of such states in real devices.

Strikingly, the SP at E_F for $t_{MgO} = 20$ ML and $T_A = 600\,^{\circ}$C has a value of almost 40%, which is a factor of two higher than for $t_{MgO} = 4$ ML. This has its origin in different properties of the outermost MgO layers, since the CMS and interface properties are the same for all samples. This is evidenced by a large work-function difference $\Delta\Phi$ of 0.7 eV, as depicted in the left part of Fig. 3, since Φ is a unique property of the surface. Therefore, we attribute the decreased SP in the case of thinner MgO coverage to additional non-spin-conserving scattering at surface defects and adsorbed molecules, which were discussed in the previous sections.

Additionally, T_A-dependent studies are performed in the interesting temperature regime of 400–600 °C. Table I gives an overview of the work-function values and the measured spin polarization (averaged over the energy range from E_F down to 0.3 eV below) for all samples investigated by SR-PES, together with the respective MgO surface defect density already reported in the previous sections. Spectra (not shown) and resulting SP do not change in the case of $t_{MgO} =$ 20 ML, as was the case for the observed LEED patterns in Sec. V. Quite contrary, both samples with intermediate MgO coverage (t_{MgO} = 6 and 10 ML) show a monotonic but rather small work-function increase by, in total, 0.35 and 0.15 eV, again in correspondence to our observations made by LEED. While the 6 ML sample also shows increased SP values near E_F due to annealing, the SP of the 10 ML sample stays constant within the error bars, similarly to the 20 ML sample (cf. Table I). The sample with the thinnest MgO top layer ($t_{MgO} = 4$ ML), however, shows further enhanced dependence

TABLE I. Qualitative amount of MgO surface defects as detected by AES and LEED, work function Φ ($\pm$0.05 eV), and spin polarization ($\pm$5%) averaged over an energy range of 300 meV below E_F in dependence upon the MgO top layer thickness t_{MgO} and the respective annealing temperature T_A. The sample with $t_{MgO} = 50$ ML is neglected as charging effects hindered the photoemission experiments.

t_{MgO} (ML)	T_A (°C)	Defect density	Φ (eV)	SP (%)
4	400	very high	2.25	–
4	500	very high	3.55	9
4	600	very high	4	16
6	400	high	3.35	20
6	600	medium	3.7	29
10	400	high	3.4	35
10	500	medium	3.55	33
10	600	medium	3.55	32
20	400	low	3.3	34
20	500	low	3.3	32
20	600	low	3.3	35

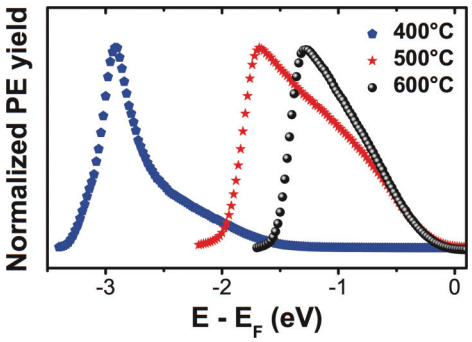

FIG. 4. (Color online) Spin-integrated and normalized spectra for $t_{MgO} = 4$ ML in dependence of T_A.

on the annealing temperature, which is shown in Fig. 4. For $T_A = 400\,^{\circ}$C, the spectrum is that of an insulator with a complete absence of photoemission yield down to 1.5 eV below E_F. We explain this as follows: Despite the annealing procedure, the presence of very high defect density at the MgO surface, which at such very low MgO thickness is strongly correlated with the defect density in the MgO film as well as at the CMS/MgO interface, leads to highly augmented inelastic electron scattering. Due to this fact, we effectively probe only the MgO layer and not the CMS/MgO interface. Elevating the annealing temperature to 500 °C, a huge work-function increase of 1.3 eV occurs as well as a finite photoemission yield near E_F, which now allows one to determine the spin polarization at the Fermi energy. Obviously, the annealing process induces defect healing, improving the interface and surface properties. Higher annealing to the optimum value of 600 °C only results in a further increase of Φ by 0.45 eV, while the SP does not change anymore. Here we want to recall that no LEED pattern could be obtained for this sample. To conclude, such drastic changes regarding the photoemission spectra do not appear at the samples with $t_{MgO} > 4$ ML, since the surface is less affected by interface-induced defects. This is in accordance with our AES and LEED results.

VII. SUMMARY

We have studied the formation of the Co_2MnSi/MgO interface by considering Co_2MnSi/MgO samples with variable MgO top layer thickness and annealing temperature. The distinct influence of interface defects onto the whole MgO layer is revealed by Auger electron spectroscopy and LEED for MgO thicknesses up to 10 ML, which can only partly be overcome by annealing. Low-energy SR-PES was used to determine the spin polarization of the CMS/MgO interface buried below the MgO layers with thickness up to 20 ML, finding distinct positive spin-polarization values in all cases. The photoemission results obtained for different annealing temperatures fully agree with the findings made by AES and LEED.

ACKNOWLEDGMENT

The authors want to gratefully acknowledge financial support through the DFG Research Unit 1464 ASPIMATT. The work at Hokkaido University was partly supported by a Grant-in-Aid for Scientific Research (A) (Grant No. 23246055) from MEXT, Japan.

*rfetzer@rhrk.uni-kl.de

[1] J. S. Moodera, Lisa R. Kinder, Terrilyn M. Wong, and R. Meservey, Phys. Rev. Lett. **74**, 3273 (1995).

[2] Evgeny Y. Tsymbal, Oleg N. Mryasov, and Patrick R. LeClair, J. Phys.: Condens. Matter **15**, R109 (2003).

[3] Igor Zutic, Rev. Mod. Phys. **76**, 323 (2004).

[4] J. P. Velev, P. A. Dowben, E. Y. Tsymbal, S. J. Jenkins, and A. N. Caruso, Surf. Sci. Rep. **63**, 400 (2008).

[5] M. Julliere, Phys. Lett. A **54**, 225 (1975).

[6] P. J. Brown, K. U. Neumann, P. J. Webster, and K. R. A. Ziebeck, J. Phys.: Condens. Matter **12**, 1827 (2000).

[7] S. Kämmerer, A. Thomas, A. Hutten, and G. Reiss, Appl. Phys. Lett. **85**, 79 (2004).

[8] T. Ishikawa, T. Marukame, H. Kijima, K. I. Matsuda, T. Uemura, M. Arita, and M. Yamamoto, Appl. Phys. Lett. **89**, 192505 (2006).

[9] S. Ishida, T. Masaki, S. Fujii, and S. Asano, Physica B: Condens. Matter **245**, 1 (1998).

[10] Benjamin Balke, Gerhard H. Fecher, Hem C. Kandpal, Claudia Felser, Keisuke Kobayashi, Eiji Ikenaga, Jung-Jin Kim, and Shigenori Ueda, Phys. Rev. B **74**, 104405 (2006).

[11] Stanislav Chadov, Gerhard H. Fecher, Claudia Felser, Jan Minar, Jürgen Braun, and Hubert Ebert, J. Phys. D **42**, 084002 (2009).

[12] Y. Sakuraba, T. Miyakoshi, M. Oogane, Y. Ando, A. Sakuma, T. Miyazaki, and H. Kubota, Appl. Phys. Lett. **89**, 052508 (2006).

[13] Takayuki Ishikawa, Naoki Itabashi, Tomoyuki Taira, Ken ichi Matsuda, Tetsuya Uemura, and Masafumi Yamamoto, Appl. Phys. Lett. **94**, 092503 (2009).

[14] Y. Sakuraba, M. Hattori, M. Oogane, Y. Ando, H. Kato, A. Sakuma, T. Miyazaki, and H. Kubota, Appl. Phys. Lett. **88**, 192508 (2006).

[15] T. Ishikawa, S. Hakamata, K. Matsuda, T. Uemura, and M. Yamamoto, J. Appl. Phys. **103**, 07A919 (2008).

[16] W. H. Butler, X.-G. Zhang, T. C. Schulthess, and J. M. MacLaren, Phys. Rev. B **63**, 054416 (2001).

[17] Y. Miura, H. Uchida, Y. Oba, K. Nagao, and M. Shirai. J. Phys.: Condens. Matter **19**, 365228 (2007).

[18] T. Ishikawa, H. Liu, T. Taira, K. Matsuda, T. Uemura, and M. Yamamoto, Appl. Phys. Lett. **95**, 232512 (2009).

[19] K. J. Chang and Marvin L. Cohen, Phys. Rev. B **30**, 4774 (1984).

[20] Yong-Nian Xu and W. Y. Ching, Phys. Rev. B **43**, 4461 (1991).

[21] D. M. Roessler and W. C. Walker, Phys. Rev. **159**, 733 (1967).

[22] Ravindra Pandey, J. E. Jaffe, and A. Barry Kunz, Phys. Rev. B **43**, 9228 (1991).

[23] Andrew Gibson, Roger Haydock, and John P. LaFemina, Phys. Rev. B **50**, 2582 (1994).

[24] L. N. Kantorovich, J. M. Holender, and M. J. Gillan, Surf. Sci. **343**, 221 (1995).

[25] Francesc Illas and Gianfranco Pacchioni, J. Chem. Phys. **108**, 7835 (1998).

[26] Ven-Chung Lee and How-Sen Wong, J. Phys. Soc. Jpn. **45**, 895 (1978).

[27] U. Schönberger and F. Aryasetiawan, Phys. Rev. B **52**, 8788 (1995).

[28] P. G. Mather, J. C. Read, and R. A. Buhrman, Phys. Rev. B **73**, 205412 (2006).

[29] Martin Sterrer, Esther Fischbach, Markus Heyde, Niklas Nilius, Hans-Peter Rust, Thomas Risse, and Hans-Joachim Freund, J. Phys. Chem. B **110**, 8665 (2006).

[30] V. V. Afanas'ev, A. Stesmans, K. Cherkaoui, and P. K. Hurley, Appl. Phys. Lett. **96**, 052103 (2010).

[31] M. Klaua, D. Ullmann, J. Barthel, W. Wulfhekel, J. Kirschner, R. Urban, T. L. Monchesky, A. Enders, J. F. Cochran, and B. Heinrich, Phys. Rev. B **64**, 134411 (2001).

[32] Y. S. Dedkov, M. Fonin, U. Rüdiger, and G. Güntherodt, Appl. Phys. A **82**, 489 (2006).

[33] Toyoo Miyajima, Mikihiko Oogane, Yasutoshi Kotaka, Takashi Yamazaki, Mineharu Tsukada, Yuji Kataoka, Hiroshi Naganuma, and Yasuo Ando, Appl. Phys. Express **2**, 093001 (2009).

[34] T. Saito, T. Katayama, T. Ishikawa, M. Yamamoto, D. Asakura, and T. Koide. Appl. Phys. Lett. **91**, 262502 (2007).

[35] Martin Jourdan, Elena Arbelo Jorge, Christian Herbort, Michael Kallmayer, Peter Klaer, and Hans-Joachim Elmers, Appl. Phys. Lett. **95**, 172504 (2009).

[36] Y. Sakuraba, K. Takanashi, Y. Kota, T. Kubota, M. Oogane, A. Sakuma, and Y. Ando, Phys. Rev. B **81**, 144422 (2010).

[37] S. Valeri, S. Altieri, A. di Bona, C. Giovanardi, and T. S. Moia, Thin Solid Films **400**, 16 (2001).

[38] J. L. Vassent, M. Dynna, A. Marty, B. Gilles, and G. Patrat, J. Appl. Phys. **80**, 5727 (1996).

[39] M. Dynna, J. L. Vassent, A. Marty, and B. Gilles, J. Appl. Phys. **80**, 2650 (1996).

[40] W. Wulfhekel, M. Klaua, D. Ullmann, F. Zavaliche, J. Kirschner, R. Urban, T. Monchesky, and B. Heinrich, Appl. Phys. Lett. **78**, 509 (2001).

[41] W. H. Wang, M. Przybylski, W. Kuch, L. I. Chelaru, J. Wang, Y. F. Lu, J. Barthel, H. L. Meyerheim, and J. Kirschner, Phys. Rev. B **71**, 144416 (2005).

[42] Jan-Peter Wüstenberg, Roman Fetzer, Martin Aeschlimann, Mirko Cinchetti, Jan Minár, Jürgen Braun, Hubert Ebert, Takayuki Ishikawa, Tetsuya Uemura, and Masafumi Yamamoto, Phys. Rev. B **85**, 064407 (2012).

[43] M. Cinchetti, J.-P. Wüstenberg, M. S. Albaneda, F. Steeb, A. Conca, M. Jourdan, and M. Aeschlimann, J. Phys. D: Appl. Phys. **40**, 1544 (2007).

[44] H. Schneider, G. Jakob, M. Kallmayer, H. J. Elmers, M. Cinchetti, B. Balke, S. Wurmehl, C. Felser, M. Aeschlimann, and H. Adrian, Phys. Rev. B **74**, 174426 (2006).

[45] J.-P. Wüstenberg, J. Fischer, C. Herbort, M. Jourdan, M. Aeschlimann, and M. Cinchetti, J. Phys. D: Appl. Phys. **42**, 084016 (2009).

[46] M. Kolbe, S. Chadov, E. Arbelo Jorge, G. Schönhense, C. Felser, H.-J. Elmers, M. Kläui, and M. Jourdan, Phys. Rev. B **86**, 024422 (2012).

[47] M. Cinchetti, J. P. Wüstenberg, and M. Aeschlimann, *Characterization of the Surface Electronic Properties of* $Co_2Cr_{1-x}Fe_xAl$ *in Spintronics: From Materials to Devices* (Springer, Dordrecht, Heidelberg, New York, London, 2013).

[48] M. Sicot, S. Andrieu, P. Turban, Y. Fagot-Revurat, H. Cercellier, A. Tagliaferri, C. De Nadai, N. B. Brookes, F. Bertran, and F. Fortuna, Phys. Rev. B **68**, 184406 (2003).

[49] F. Matthes, L.-N. Tong, and C. M. Schneider, J. Appl. Phys. **95**, 7240 (2004).

[50] Martina Müller, Frank Matthes, and Claus M. Schneider, J. Appl. Phys. **101**, 09G519 (2007).

[51] Liu-Niu Tong, Cai-Lian Deng, Frank Matthes, Martina Müller, Claus M. Schneider, and Chan-Gyu Lee, Phys. Rev. B **73**, 214401 (2006).

[52] F. Bonell, T. Hauet, S. Andrieu, F. Bertran, P. Le Fèvre, L. Calmels, A. Tejeda, F. Montaigne, B. Warot-Fonrose, B. Belhadji,

A. Nicolaou, and A. Taleb-Ibrahimi, Phys. Rev. Lett. **108**, 176602 (2012).

[53]L. Plucinski, Y. Zhao, B. Sinkovic, and E. Vescovo, Phys. Rev. B **75**, 214411 (2007).

[54]R. Fetzer, J.-P. Wüstenberg, T. Taira, T. Uemura, M. Yamamoto, M. Aeschlimann, and M. Cinchetti, arXiv:1209.4368.

[55]Masafumi Yamamoto, Takayuki Ishikawa, Tomoyuki Taira, Gui fang Li, Ken ichi Matsuda, and Tetsuya Uemura, J. Phys.: Condens. Matter **22**, 164212 (2010).

[56]M. Yamamoto, T. Marukame, T. Ishikawa, K. Matsuda, T. Uemura, and M. Arita, J. Phys. D: Appl. Phys. **39**, 824 (2006).

[57]L. Davis, N. MacDonald, P. Palmberg, and G. Riach. *Handbook of Auger Electron Spectroscopy: A Reference Book of Standard Data for Identification and Interpretation of Auger Electron Spectroscopy Data* (Physical Electronics, Eden Prairie, Minnesota, 1987).

[58]J. Hermanson, Solid State Commun. **22**, 9 (1977).

[59]A. Jablonski and C. J. Powell. NIST Electron Inelastic-Mean-Free-Path Database, Technical Report No. 71, National Institute of Standards and Technology, 2000 (unpublished).

[60]Victor Henrich, Rep. Prog. Phys. **48**, 1481 (1985).

[61]Gregory Geneste, Joseph Morillo, and Fabio Finocchi, J. Chem. Phys. **122**, 174707 (2005).

[62]D. Ochs, M. Brause, B. Braun, W. Maus-Friedrichs, and V. Kempter, Surf. Sci. **397**, 101 (1998).

[63]Gianfranco Pacchioni, Josep M. Ricart, and Francesc Illas, J. Am. Chem. Soc. **116**, 10152 (1994).

[64]Gianfranco Pacchioni, Surf. Sci. **281**, 207 (1993).

[65]Gianfranco Pacchioni, Tommaso Minerva, and Paul S. Bagus, Surf. Sci. **275**, 450 (1992).

[66]M. J. Gillan, L. N. Kantorovich and J. A. White, J. Chem. Soc., Faraday Trans. **92**, 2075 (1996).

[67]L. N. Kantorovich and M. J. Gillan, Surf. Sci. **374**, 373 (1997).

[68]Ming-Cheng Wu, Jason S. Corneille, Cesar A. Estrada, Jian-Wei He, and D. Wayne Goodman, Chem. Phys. Lett. **182**, 472 (1991).

[69]C. Tegenkamp, H. Pfnür, W. Ernst, U. Malaske, J. Wollschläger, D. Peterka, K. M. Schröder, V. Zielasek, and M. Henzler, J. Phys.: Condens. Matter **11**, 9943 (1999).

[70]Y. Miura, H. Uchida, Y. Oba, K. Abe, and M. Shirai, Phys. Rev. B **78**, 064416 (2008).

[71]Björn Hülsen, Matthias Scheffler, and Peter Kratzer, Phys. Rev. B **79**, 094407 (2009).